Geophys. J. Int. (2012) **190,** 293–309 doi: 10.1111/j.1365-246X.2012.05470.x

Using empirical mode decomposition to process marine magnetotelluric data

Jin Chen,[1] Bjoern Heincke,[1] Marion Jegen[1] and Max Moorkamp[1,2]

[1]*GEOMAR, Wischhofstrasse* 1-3, 24148 *Kiel, Germany. E-mail: jchen@geomar.de*
[2]*Department of Geology, University of Leicester, Leicester* LE1 7RH, *UK*

Accepted 2012 March 21. Received 2012 March 16; in original form 2011 April 22

SUMMARY

A major step in processing magnetotelluric (MT) data is the calculation of an impedance tensor as function of frequency from recorded time-varying electromagnetic fields. Common signal processing techniques such as Fourier transform based procedures assume that the signals are stationary over the record length, which is not necessarily the case in MT, due to the possibility of sudden spatial and temporal variations in the naturally occurring source fields. In addition, noise in the recorded electric and magnetic field data may also be non-stationary. Many modern MT processing techniques can handle such non-stationarities through strategies such as windowing of the time-series. However, it is not completely clear how extreme non-stationarity may affect the resulting impedances. As a possible alternative, we examine a heuristic method called empirical mode decomposition (EMD) that is developed to handle arbitrary non-stationary time-series. EMD is a dynamic time series analysis method, in which complicated data sets can be decomposed into a finite number of simple intrinsic mode functions.

In this paper, we use the EMD method on real and synthetic MT data. To determine impedance tensor estimates we first calculate instantaneous frequencies and spectra from the intrinsic mode functions and apply the impedance formula proposed by Berdichevsky to the instantaneous spectra. We first conduct synthetic tests where we compare the results from our EMD method to analytically determined apparent resistivities and phases. Next, we compare our strategy to a simple Fourier derived impedance formula and the frequently used robust processing technique bounded-influence remote reference processing (BIRRP) for different levels of stochastic noise. All results show that apparent resistivities and phases which are calculated from EMD derived impedance tensors are generally more stable than those determined from simple Fourier analysis and only slightly worse than those from the robust processing. These results show that EMD has the potential to handle noisy data. Finally, as a test on real data, we apply our processing scheme to data measured from the Costa Rica subduction zone, and obtain similar impedance estimates as the BIRRP processing method.

Key words: Time-series analysis; Magnetotelluric.

1 INTRODUCTION

Magnetotelluric (MT) studies use natural electromagnetic source fields generated in the ionosphere and magnetosphere as a source which is assumed to be quasi-uniform. The horizontal components of these time-varying electric and magnetic fields are measured at the Earth's surface and their spectral ratio gives the impedance as a function of frequency. This impedance can be used to determine the conductivity structure in the subsurface. In standard MT data processing routines, the Fourier transform is used to determine the spectra (e.g. Sims *et al.* 1971; Vozoff 1972) and impedance estimates are determined through a combination of methods like remote reference (e.g. Gamble *et al.* 1979a,b), multitaper spectral analysis (Thomson 1982), robust estimates (e.g. Egbert & Booker 1986; Chave & Thomson 1989) and bounded-influence remote reference processing, BIRRP (Chave & Thomson 2004). In particular, the latter modern MT processing codes have greatly improved the reliability of impedance calculations. They also address non-stationarity and noise problems through windowing the times series into shorter segments and combining them such that anomalous segments are removed in the impedance estimate. However, sometimes even sophisticated methods can provide poorly determined impedance estimates (Szarka 1988; Qian & Pedersen 1991).

The main reason for these problems is that in practice, field data contains signal components which violate the source assumption made in MT processing. Electromagnetic signals measured on land may be contaminated by artificial noise originating from, for example power

lines, electrical fences and other industrial sources (Szarka 1988; Junge 1996). In addition, high power transients with a distinct non-stationary behaviour are often present. Marine measurements are often noisy because of the surface waves, passing ships and the noise associated with tilt movements of the MT instruments. Because these signal components are usually present in both the electric and magnetic fields, they cause high coherence in the associated time-series and may be difficult to remove by standard processing techniques. Therefore, noisy sections of the time-series are typically removed before processing. For low quality data this means that only a small portion of data may remain for impedance calculation.

Furthermore, one underlying assumption for methods using power spectral densities calculated through Fourier analysis is that the time-series are in a wide-sense stationary. However, many geomagnetic time-series recorded for MT investigations are characterized by a changing frequency content with time mainly due to contamination by transient local natural or artificial noise signals, and can be considered as non-stationary within typical recording lengths (Chant & Hastie 1992, 1993). If a non-stationary event is present in the time section many additional harmonic components are needed to describe this event. This is particularly true if the non-stationary event has an impulsive character. As a result, the energy is then spread over a wide frequency range. Constrained by energy conservation, these spurious harmonics and the wide frequency spectrum cannot faithfully represent the true energy density in frequency space (Huang *et al.* 1998). Chant & Hastie (1992, 1993) demonstrate on MT field data that the impedance tensor is affected significantly by such non-stationary source field fluctuations when using Fourier transform based processing.

To process non-stationary MT signals, Chant & Hastie (1992, 1993) use time-frequency distribution (TFD) analysis techniques that give energy distributions of the signals both in frequency and time and provide stable and reliable impedance estimates through an evolutive estimate. However estimates from TFD techniques are still considered as problematic since they are affected by the complexity of MT signals, and, depending on the signal character, different time-lag kernel function are considered as appropriate (Chant & Hastie 1992). Wavelet analysis is a different approach to handle non-stationary data and has become a standard data analysis method (e.g. Alexandrescu *et al.* 1995; Suto *et al.* 2006; Garcia & Jones 2008). However, since wavelet analysis gives time-frequency information over time-variable windows, a wavelet basis that is suited for all signals in the time-series has to be selected before processing. Moreover, wavelet analysis has typically relatively low frequency resolution (Huang *et al.* 1998). Robust processing techniques (Chave & Thomson 2004) can also handle non-stationary data by adapting the segment lengths in time to the frequencies of interest. Such techniques have, moreover, the advantage that their bias and statistical properties are well developed. Another way to address the problem of non-stationarity is to use instantaneous frequency (IF) and instantaneous amplitude (IA), which are not based on the decomposition of the time-series into fixed basis functions and allow for imaging the frequency content as a function of time. However, calculation of IF is only physically meaningful when the signal is mono-component, which means that the signal is zero-mean and amplitude & frequency modulated (AM-FM) (Boashash 1992a,b; Loughlin & Tracer 1996; Huang *et al.* 2009). Since geomagnetic time-series, like most other time-series, typically are not mono-component, IFs directly calculated from these time-series are generally not physically meaningful.

With the development of the empirical mode decomposition (EMD) introduced by Huang *et al.* (1998), a processing method exists which decomposes non-stationary time-series into a sequence of mono-component signals, termed intrinsic mode functions (IMFs). Accordingly, physically meaningful instantaneous frequencies can be calculated for all IMFs. Compared to traditional Fourier analysis, EMD works directly in the time domain rather than in frequency domain and results are typically presented as time-frequency-energy representations. However, due to its definition, EMD is an empirical method in contrast to the mathematically well-defined Fourier transform.

Over the last 10 yr, the heuristic EMD approach has demonstrated its applicability in a wide range of geoscience studies, as well as in many other different research fields. For instance, Vasudevan & Cook (2000) use EMD to extract the scaling behaviour of reflected waves. Huang *et al.* (2001) apply EMD to seismic time-series from a large earthquake and conclude that Fourier analysis seriously under-represents low frequency energy due to artificial high frequency harmonics. Zhang *et al.* (2003a,b) and (Zhang 2006) use EMD in tracing seismic wave propagation. Applications of EMD in meteorological studies have been summarized by Duffy (2004) and Huang & Wu (2008) give a review of applications in atmosphere, climate and oceanographic studies.

In this paper we investigate how EMD, combined with instantaneous spectra calculation is suited for the processing of marine MT data, which is typically characterized by non-stationary noise. In this context we apply the procedure to both synthetic and field data. The MT data sets are first decomposed into intrinsic mode functions using EMD. Then we calculate instantaneous frequencies of each intrinsic mode function through an empirical amplitude and frequency demodulation method proposed by Huang *et al.* (2009). Finally, the obtained time-frequency distributions are used for impedance estimation. In contrast to traditional processing, the impedance estimation is performed in the time-frequency-domain using instantaneous spectra (Berdichevsky 1973) rather than in the frequency domain. To evaluate the results we compare our impedance estimates to analytical results for the case of synthetic data, and with estimates from a standard MT data processing technique (Chave & Thomson 2004) for the case of real data example. For the synthetic data we moreover investigate, how stable the impedance estimates are in the presence of stochastic noise.

In this paper we first introduce the EMD method. Based on a simple example, we show how to apply the EMD to a time-series to obtain intrinsic mode functions and illustrate the concepts of instantaneous amplitude, instantaneous frequency and instantaneous spectrum. We use the direct quadrature (Huang *et al.* 2009) and not the traditional analytic signal based on Hilbert transform to calculate more accurate instantaneous frequencies from the IMFs. We then present the theory of impedance estimation when signals are represented as instantaneous spectra in the time domain. By means of a synthetic layered Earth model we test our estimation procedure. Finally, we apply the same procedure to a marine MT field data set and compare our results with the ones obtained from processing the data with BIRRP (Chave & Thomson 2004).

2 METHODOLOGY

2.1 Empirical model decomposition

Huang *et al.* (1998) introduced empirical mode decomposition (EMD) as a new non-stationary data processing method. It is based on an adaptive procedure to decompose non-stationary signals into IMFs and a monotonic residue. The adaptive decomposition maintains the local signal characteristics and guarantees that the signals in all IMFs are mono-component. As mono-component signals allow the calculation of physically meaningful instantaneous frequencies, any event in the signal can hence be localized on the time axis as well as the frequency axis by presenting the IMFs in frequency-time-energy distributions. This is particularly relevant for processing of non-stationary time-series, since instantaneous frequencies and energies are more useful than globally determined frequencies and energies, like those obtained from Fourier spectral analysis. Although the calculation procedures are very different for EMD and Fourier analysis, we emphasize that EMD is also an expansion into basis functions and considered by Huang *et al.* (1998) as a generalization of the Fourier transform.

In order to obtain physical meaningful IFs, the IMFs have to satisfy two conditions (Huang *et al.* 1998; Rilling *et al.* 2003; Flandrin 2004):

(1) in each IMF, the number of extrema and the number of zero crossings must either equal or differ at most by one, and
(2) at any time, the mean value of the envelopes determined from the local maxima and the local minima of each IMF is zero.

Considering these two conditions the IMFs can be associated with simple oscillatory modes that are embedded in the time-series. The procedure to decompose signals with EMD differs substantially from the one of Fourier analysis. Based on these two conditions, a signal $x(t)$ is decomposed into IMFs through an iterative process termed 'sifting' (Huang *et al.* 1998; Rilling *et al.* 2003; Flandrin 2004) that is described in the following:

(1) Identify all local extrema of $x(t)$.
(2) Interpolate all local maxima and local minima by cubic splines to obtain upper and lower envelopes, respectively.
(3) Subtract the mean $m_{11}(t)$ of the upper and lower envelopes from $x(t)$ to obtain the signal $h_{11}(t) = x(t) - m_{11}(t)$.
(4) If $h_{11}(t)$ fulfills the two conditions mentioned above to a predefined numerical precision, it is considered as the first IMF $c_1(t) = h_{11}(t)$. Otherwise, steps 1–3 are applied on $h_{11}(t)$ (instead of $x(t)$) and are repeated $i - 1$ times until $h_{1i} = h_{1(i-1)}(t) - m_{1i}(t)$ fulfills the conditions. $c_1(t) = h_{1i}(t)$ is then considered as the first IMF.
(5) Subtract the first IMF $c_1(t)$ from $x(t)$ and treat the obtained signal as a new time-series $\tilde{x}(t) = x(t) - c_1(t)$.

Steps 1 to 5 are repeated to determine the subsequent IMFs $c_j(t)$ from the remaining signal $\tilde{x}(t)$. The decomposition process is stopped after n iterations when the residue becomes a monotonic function r_n ,which can not be decomposed further. The final signal can then be expressed as a sum of all IMFs and the residual:

$$x(t) = \sum_{j=1}^{n} c_j + r_n. \tag{1}$$

The sum of all IMFs and the residual completely recovers the signal. The IMFs contain different frequency bands, where the highest frequencies are usually found in the first IMF and lower frequencies in subsequent IMFs. The number of IMFs needed to represent the non-stationary signal depends on the complexity of the signal. In this context, Wu & Huang (2004) mention that EMD works as a dyadic filter for white noise resulting in a number of IMFs close to $log2(N)$, where N is the number of samples.

EMD has a number of limitations that are tied to the assumptions needed to implement the algorithm. First of all, it is theoretically not guaranteed that the IMFs are exactly orthogonal. Although Huang *et al.* (1998) concluded that the orthogonality is typically satisfied in a practical sense, other researchers (see Huang *et al.* 2008)[1] state that the lack of total orthogonality can be responsible for energy leakage in the sifting process and is not negligible. However, Huang *et al.* (2008) proposed a modification of the EMD method called OEMD (orthogonal empirical mode decomposition) that guarantees complete orthogonality of the IMFs. We have not implemented this modification yet but instead we attempt to quantify the orthogonality numerically based on two criteria proposed by Huang *et al.* (1998):

(i) The overall index of orthogonality, *IO*, defined as

$$IO = \sum_{t} \left(\sum_{j=1, j\neq k}^{n+1} \sum_{k=1}^{n+1} c_j(t) c_k(t) / x^2(t) \right) \tag{2}$$

and

(ii) orthogonality for any two components

$$IO_{jk} = \sum_{t} \frac{c_j(t) c_k(t)}{c_j^2(t) + c_k^2(t)}. \tag{3}$$

[1] The name of the first author is Tian-li Huang. He is not the same person as Norden Huang, who first proposed EMD.

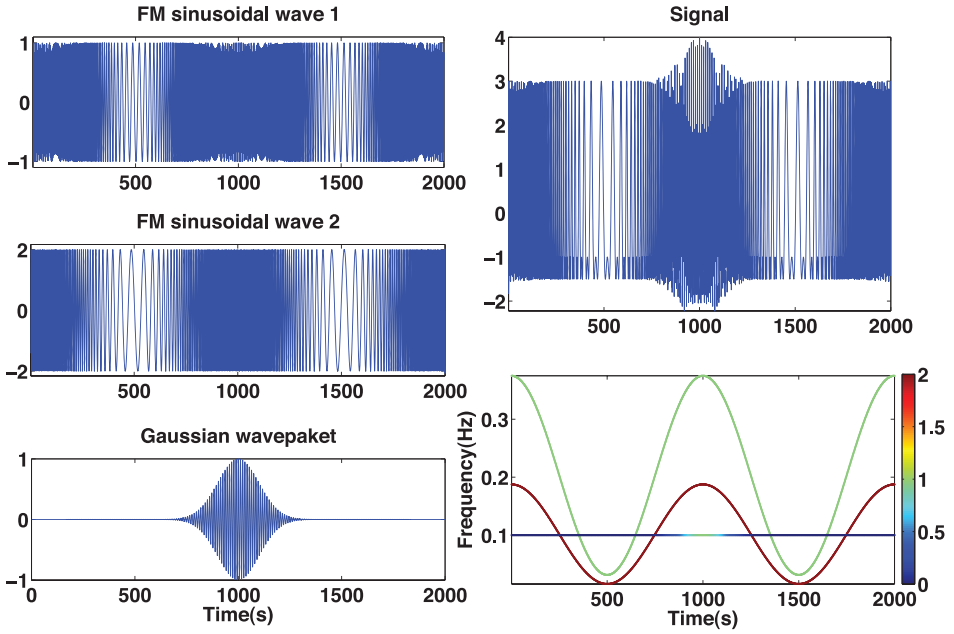

Figure 1. Synthetic time-series (right upper panel) consisting of three components: two sinusoidal FM signals with amplitude levels of 1 and 2, respectively, and a Gaussian wavepacket (left panels). The frequency variation with time for the three components are shown in the right lower panel. The colours indicate the associated amplitudes.

The first criteria can vary from 0.0 to 1.0 and the second criteria can vary from 0.0 to 0.5. Zero values for the first criteria indicate that the IMFs span a perfectly orthogonal system. Zero values for the second criteria shows that the associated two IMFs are orthogonal.

A second problem is that the iterative sifting process introduces numerical inaccuracies (Rato *et al.* 2008).

(1) Due to the numerical stop criteria used in the sifting process, the average of the upper and lower envelopes is not exactly the true mean of a signal and therefore the IMFs are not exactly zero mean signals (Huang *et al.* 1998; Rilling *et al.* 2003; Flandrin 2004).

(2) The IMFs show some inaccuracies at the boundaries (e.g. Flandrin 1999; Rato *et al.* 2008). To reduce these effects one or two more maxima/minima values at the boundaries are usually mirrored. After comparing several strategies, we choose the extrapolation strategy of Rato *et al.* (2008).

To illustrate how the EMD method works we use a synthetic time-series (modified from Rilling *et al.* (2003)) sampled at 10 Hz which contains three components: two sinusoidal frequency modulated waves with amplitudes 1 and 2, respectively, and a Gaussian wavepacket. Fig. 1 shows the three components (left three panels) of the time-series (right upper panel) and their frequency contents as a function of time (right lower panel). First, we use a discrete prolate spheroidal sequence with a time-bandwidth of 1 as tapering window and overlapping sections (Chave *et al.* 1987) to robustly estimate the power spectra for the three time-series, as shown in Fig. 2.

Because the Fourier spectra of the three time-series are overlapping in frequency domain, it will be not possible to separate the signal characteristics of the individual components by Fourier transform. Accordingly, Fourier analysis cannot decompose the time-series in a way that physically meaningful instantaneous frequencies can be reconstructed as we will show below.

When applying EMD to the signal instead, 11 IMFs are obtained from which the first six IMFs are shown in Fig. 3. A change of frequency content from high to low frequencies can be observed with increasing order of the IMF components. The first two IMFs mainly contain the signals from the two frequency modulated components and the third IMF mainly contains the signals from the Gaussian wavepacket. The remaining eight IMFs have comparably small amplitudes and are induced by the numerical procedure for estimating the IMFs. As mentioned before, the sum of the 11 IMFs completely recovers the original signal. Moreover, low values of 0.0190 for the overall index of orthogonality *IO* (see eq. 2) and low values for the components of the orthogonality matrix (see eq. 3) for the first four IMFs shown in Table 1 indicate that the IMFs represent, to a first approximation, an orthogonal system.

The above example has demonstrated how the EMD method decomposes a multicomponent signal into mono-component functions. In the next section we introduce the concepts of instantaneous frequency and amplitude and illustrate its meaning by means of this synthetic time-series example.

2.2 Instantaneous frequency and amplitude

As shown above, the traditional Fourier method based on global frequency content and energy distribution may not be suitable for non-stationary processes. In this context the concept of instantaneous frequencies and amplitudes based on local characteristics of the signal becomes very important.

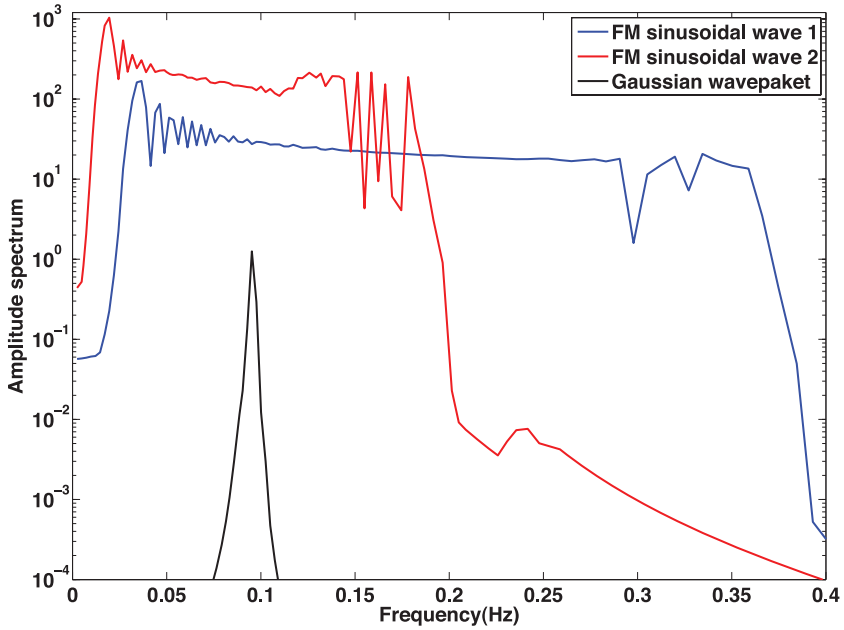

Figure 2. Fourier spectra of the three components of the synthetic time-series shown in Fig. 1. (To obtain these spectra a discrete prolate spheroidal sequence with a time-bandwidth of 1 as tapering window is applied on overlapping sections.)

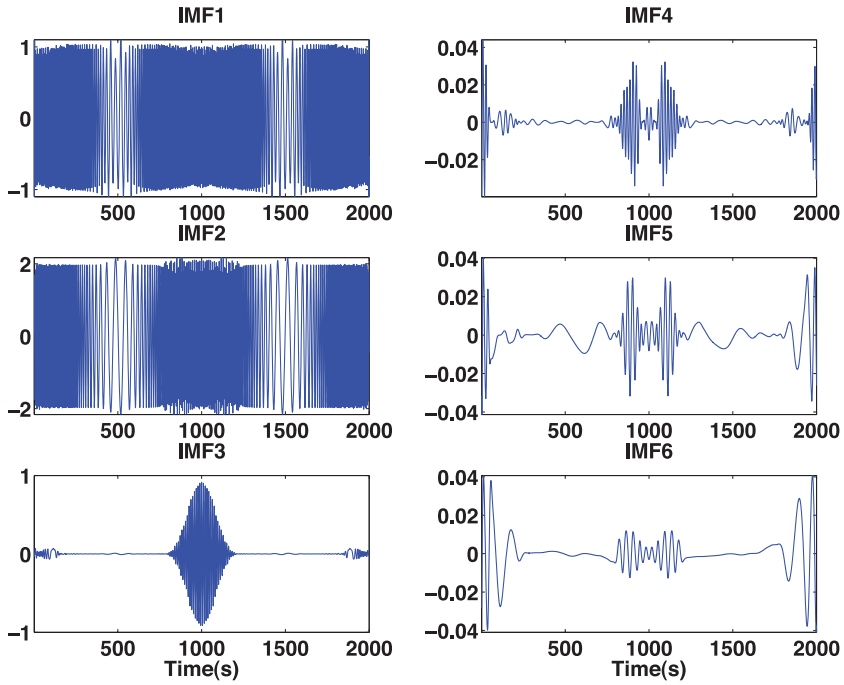

Figure 3. The first six of a total of 11 IMFs of the synthetic time-series is shown in Fig. 1. The first three IMFs (IMF1–3) have higher amplitudes. IMF1 and IMF2 mainly represent the two FM components of the signal and IMF3 mainly represents the Gaussian wavepacket (compare with Fig. 1). Relatively high amplitudes at the borders of the IMFs 4–6 are related to some boundary problems (Rato *et al.* 2008).

There are different ways to derive instantaneous frequencies (IF) and instantaneous amplitudes (IA) from a time-series. A classical approach is described by Gabor (1946) through the generation of an analytic signal, where a real valued time-series is mapped into the complex plane. In this approach the imaginary part of the analytic signal is generated through a Hilbert transform of the original time-series, such that the real time signal and its Hilbert transformation are then characterized by a phase shift of $\pi/2$.

The Hilbert transform $y(t)$ of a time-series $x(t)$ is defined as:

$$y(t) = \frac{1}{\pi} \wp \int_{-\infty}^{\infty} \frac{x(t')}{t - t'} \mathrm{d}t' \tag{4}$$

Table 1. Components of the orthogonality matrix for the first four IMFs.

IO_{ij}	c_1	c_2	c_3	c_4
c_1	0.5			
c_2	0.0156	0.5		
c_3	0.0027	0.0039	0.5	
c_4	0.0000	0.0000	0.0005	0.5

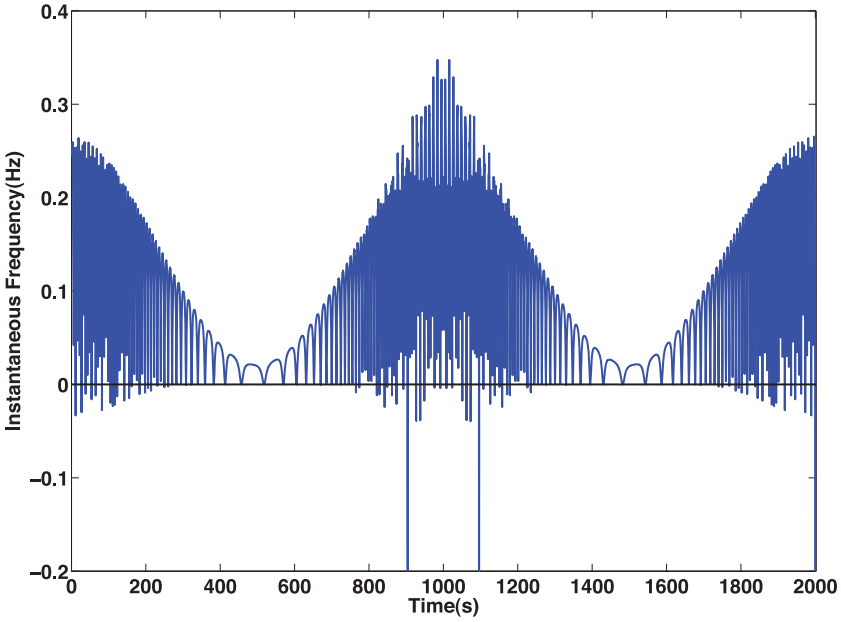

Figure 4. Instantaneous frequencies calculated from the synthetic time-series (see Fig. 1) without prior EMD decomposition. The IFs are computed from the analytic signal through the Hilbert transform. Comparison with the right lower panel in Fig. 1 shows that the derived IFs are not physically meaningful and can not be used to characterize the time-series.

where $\wp$ indicates the Cauchy principal value. A complex analytic signal $w(t)$ can then be constructed as

$$w(t) = x(t) + iy(t) = a(t)e^{i\theta(t)} \tag{5}$$

where $a(t) = \sqrt{x^2(t) + y^2(t)}$ and $\theta(t) = \text{atan}(\frac{y(t)}{x(t)})$. The instantaneous amplitude can then be defined as $a(t)$ and the instantaneous frequency as

$$\omega(t) = \frac{\mathrm{d}\theta(t)}{\mathrm{d}t}. \tag{6}$$

However, if a time-series consists of a superposition of different mono-component signals, using the above described approach to calculate the IFs and IAs is not physically meaningful. This can be easily seen in our synthetic time-series example. If we directly use the analytic signal to calculate the IFs, the instantaneous frequencies obtained, as shown in Fig. 4, vary very rapidly with time accommodating for the fact that at least two frequencies are present at each point in time. Moreover, negative instantaneous frequencies are present for a number of time samples. Obviously such a procedure does not recover the characteristics of the signal (compare frequency variations with time in Figs 1 and 4). Therefore a decomposition of the signal into mono-component functions taking into consideration non-stationary variations is needed before IFs and IAs can be calculated. The EMD method exactly does this and accordingly resolves one crucial problem for computing physically meaningful instantaneous frequencies from a multicomponent signal.

However, even for mono-component zero-mean AM-FM signals, there still are two remaining difficulties if IFs and IAs are calculated by analytic signals based on the Hilbert transform (Huang & Wu 2008; Huang *et al.* 2009). First, mono-component signals may be still composed of an amplitude modulated and a frequency modulated component. According to the Bedrosian theorem (Bedrosian 1963) meaningful spectra obtained through Hilbert transform are then only guaranteed if their associated spectra do not overlap. Second, from the Nuttall theorem (Nuttall & Bedrosian 1966) it can be concluded that for signals with complicated phase variations, the phase shift between the real and imaginary part is not necessarily $\pi/2$ if the Hilbert transform is used. Violation of these conditions can lead to physically non-meaningful instantaneous frequencies that may even be negative (Loughlin & Tracer 1996).

To avoid such exceptional cases Huang *et al.* (2009) propose to use an empirical amplitude and frequency demodulation method to calculate the IFs instead. In this method the direct quadrature and not the Hilbert transform is considered as the imaginary part of the complex time-series. Use of the direct quadrature has the advantage that the obtained IFs are guaranteed to be physically meaningful (Loughlin &

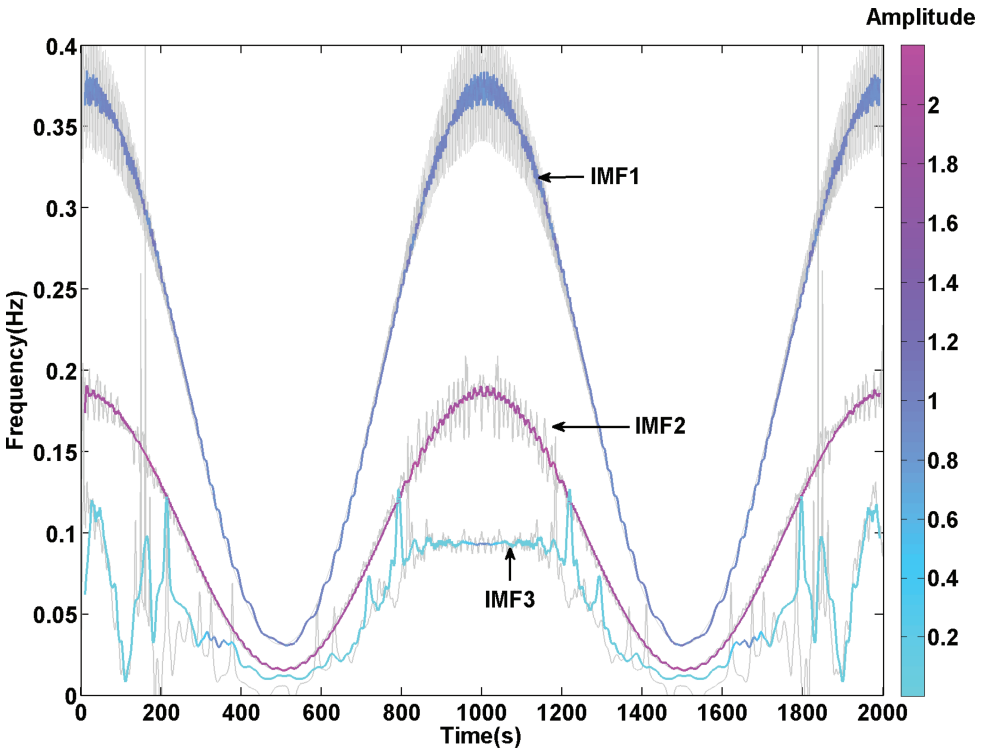

Figure 5. Instantaneous spectrum of the first three IMFs of the synthetic time-series. Instantaneous frequencies are determined by usage of the direct quadrature. Colour indicates the amplitude level. As a comparison, the thin grey lines are the IFs calculated using analytic signals based on Hilbert transform. For these Hilbert transform-based IFs no amplitude information is plotted.

Tracer 1996) provided that the signal is mono-component. The direct quadrature is now defined as follows. Assume the mono-component signal is expressed as $c(t) = a(t)\cos\phi(t)$, where $a(t)$ is the AM part and $\cos\phi(t)$ the FM part, then its quadrature is defined as $c^q(t) = a(t)\sin\phi(t)$. For the complex time-series

$$w_i(t) = c_i(t) + ic_i^q(t) \tag{7}$$

the instantaneous frequency can be calculated for each IMF in the same way as for the Hilbert transform by using eq. (6). To determine the IFs by means of the direct quadrature, Huang *et al.* (2009) propose an iterative normalization scheme that separates the IMFs uniquely into their AM and FM parts. The normalization process is set up such that the FM amplitude level becomes constant and that the zero-crossing points of the FM part are the same as for the original IMF. The normalized FM part then allows the direct computation of quadrature and satisfies the conditions both from Bedrosian's and Nuttall's theorem. A detailed description of the method is given by Huang *et al.* (2009). We test both the Hilbert transform and the empirical demodulation method to determine the IFs and observe that the IF calculation is significantly more robust and accurate using Huang's demodulation method, as shown in Fig. 5. Therefore, in the following we will only present results, where the calculation of instantaneous frequencies is performed using the direct quadrature of the signal.

After decomposing the time-series using EMD, the signal $x(t)$ can be expressed as a sum of IMFs and a residual (see eq. 1), and the instantaneous frequency $\omega_j(t)$ and amplitude $a_j(t)$ of each IMF can be calculated. If we omit the residual term, the signal can be expressed as

$$x(t) \approx \mathrm{Re}\left(\sum_{j=1}^{n} a_j(t)e^{i\omega_j(t)t}\right). \tag{8}$$

This enables us to represent the amplitude and frequency contents of the signal as functions of time. This frequency-time distribution of the amplitude is called the *instantaneous spectrum* $S(\omega, t)$. For the synthetic time-series used as an example above the instantaneous spectrum of the first three IMFs of the synthetic time-series is shown in Fig. 5. Comparison with the right lower panel in Fig. 1 clearly demonstrates that the frequency content as well as the amplitude level of the two sinusoidal frequency modulated waves and the Gaussian wavepacket are generally recovered by these IMFs. This indicates that the IMFs are mono-component and that their IFs are physically meaningful.

2.3 Magnetotelluric impedance estimates based on instantaneous spectra

We will now show how the instantaneous spectrum can be used to calculate estimates of the MT impedance tensor. Using the Fourier transform the calculation of the MT impedance tensor is, at least in theory, straightforward. The E- and B-fields time-series are transferred into the

frequency domain, and then the impedance tensor Z (Vozoff 1972)

$$\begin{pmatrix} E_x(\omega) \\ E_y(\omega) \end{pmatrix} = \frac{1}{\mu_0} \begin{pmatrix} Z_{xx}(\omega) & Z_{xy}(\omega) \\ Z_{yx}(\omega) & Z_{yy}(\omega) \end{pmatrix} \begin{pmatrix} B_x(\omega) \\ B_y(\omega) \end{pmatrix} \tag{9}$$

is determined through linear regression (Sims *et al.* 1971). One option to determine the impedances is to solve eq. (9) in a least square sense.

$$\mathbf{Z} = \mu_0(\mathbf{E}\mathbf{B}^*)(\mathbf{B}\mathbf{B}^*)^{-1} \quad , \tag{10}$$

where $*$ indicates the complex conjugate. In practice, noisy measurements make it necessary to utilize a number of sophisticated statistical methods to derive robust and reliable impedance estimates (e.g. Chave & Thomson 1989; Sutarno & Vozoff 1991; Chant & Hastie 1992; Spagnolini 1994; Egbert 1997; Lamarque 1999). We will discuss these issues in relation to our proposed method below.

However, impedances estimates derived from eq. (9) are defined purely in frequency domain and cannot be used for our instantaneous spectra obtained by the EMD. Therefore we use the formula proposed by Berdichevsky (1973) instead. He proposed an impedance tensor estimate in the time-frequency-domain, in which he decomposes the MT time-series using a series of narrow band filters around the desired estimation frequency, constructs a complex signal from each filtered time-series and obtains the following equations:

$$\begin{pmatrix} \sum_{n=0}^{N} E_{xf}(t_n)B^*_{yf}(t_n) \\ \sum_{n=0}^{N} E_{yf}(t_n)B^*_{yf}(t_n) \end{pmatrix} = \frac{1}{\mu_0} \begin{pmatrix} Z_{xx}(\omega_0) & Z_{xy}(\omega_0) \\ Z_{yx}(\omega_0) & Z_{yy}(\omega_0) \end{pmatrix} \begin{pmatrix} \sum_{n=0}^{N} B_{xf}(t_n)B^*_{yf}(t_n) \\ \sum_{n=0}^{N} B_{yf}(t_n)B^*_{yf}(t_n) \end{pmatrix} \tag{11}$$

and

$$\begin{pmatrix} \sum_{n=0}^{N} E_{xf}(t_n)B^*_{xf}(t_n) \\ \sum_{n=0}^{N} E_{yf}(t_n)B^*_{xf}(t_n) \end{pmatrix} = \frac{1}{\mu_0} \begin{pmatrix} Z_{xx}(\omega_0) & Z_{xy}(\omega_0) \\ Z_{yx}(\omega_0) & Z_{yy}(\omega_0) \end{pmatrix} \begin{pmatrix} \sum_{n=0}^{N} B_{xf}(t_n)B^*_{xf}(t_n) \\ \sum_{n=0}^{N} B_{yf}(t_n)B^*_{xf}(t_n) \end{pmatrix}, \tag{12}$$

where $E_{xf}(t)$, $E_{yf}(t)$, $B_{xf}(t)$, $B_{yf}(t)$ are the transient values of the complex signals corresponding to the frequency ω_0. The complex conjugate is denoted by $*$ and N is the number of sampling points in time domain. Actually, the two formulas from Vozoff and Berdichevsky are based on the same model and can, hence, be transformed from one to the other.

According to eqs (11)–(12), the impedance component Z_{xy} can be calculated as

$$Z_{xy} = \mu_0 \frac{\sum_{n=0}^{N} E_{xf}(t_n)B^*_{yf}(t_n) \sum_{n=0}^{N} B_{xf}(t_n)B^*_{xf}(t_n) - \sum_{n=0}^{N} E_{xf}(t_n)B^*_{xf}(t_n) \sum_{n=0}^{N} B_{xf}(t_n)B^*_{yf}(t_n)}{\sum_{n=0}^{N} B_{xf}(t_n)B^*_{xf}(t_n) \sum_{n=0}^{N} B_{yf}(t_n)B^*_{yf}(t_n) - \sum_{n=0}^{N} B_{xf}(t_n)B^*_{yf}(t_n) \sum_{n=0}^{N} B_{yf}(t_n)B^*_{xf}(t_n)} \tag{13}$$

and the other components Z_{xx}, Z_{yx}, Z_{yy} can be calculated similarly.

To construct complex signals (required for eqs 11–13) from the real valued time-series we used the direct quadratures of the IMFs as the imaginary part of the time-series (see eq. 7 and discussion above).

One practical problem in using the Berdichevsky formula is that there are rarely any frequencies ω_0 for which frequency information exists for all time samples and in all different E- and B-field components simultaneously. This is because individual IMFs have only one specific frequency value at each time sample and these IMFs typically vary with time. To make the eqs (11)–(13) applicable we therefore divide the frequency axis into a number frequency windows (see Fig. 6) and use the center frequencies of each window as the ω_0, for which impedance tensor estimates should be calculated. For each B- and E-field component we then determine for each time sample and for each IMF the frequency window into which the corresponding IMFs fall. The values are used in further processing only if a value in the frequency window is present for all components simultaneously. The associated contributions from the complex signals are summed up for all windows and all field components and the summands are finally used in eq. (13) to estimate the impedance tensor elements for the associated center frequency ω_0. In the following section we will see that such an approximation is adequate for impedance calculation as long as the size of the frequency windows are not too large, since impedances only vary gradually with frequencies.

3 SYNTHETIC MODEL TEST

As a first test we apply the new method to synthetic data with a known impedance Z. We use a synthetic three layered Earth model as shown in Fig. 7 to construct the time-series. We chose such an Earth model with large resistivity contrasts in order to produce an apparent resistivity curve with strong slopes that give clear indication whether our estimated impedance values are correct.

We use 9 d of measured B-field time-series with a sampling frequency of 1 Hz recorded in Costa Rica in 2007 (Fig. 8.) as the synthetic magnetic field time-series. To construct synthetic E-field data, impedances $Z(\omega)$ are calculated from our simple 1-D model and the B-field time-series are transferred to the frequency domain by using the Fourier transform. Then the impedance $Z(\omega)$ is multiplied with $B_y(\omega)$ and

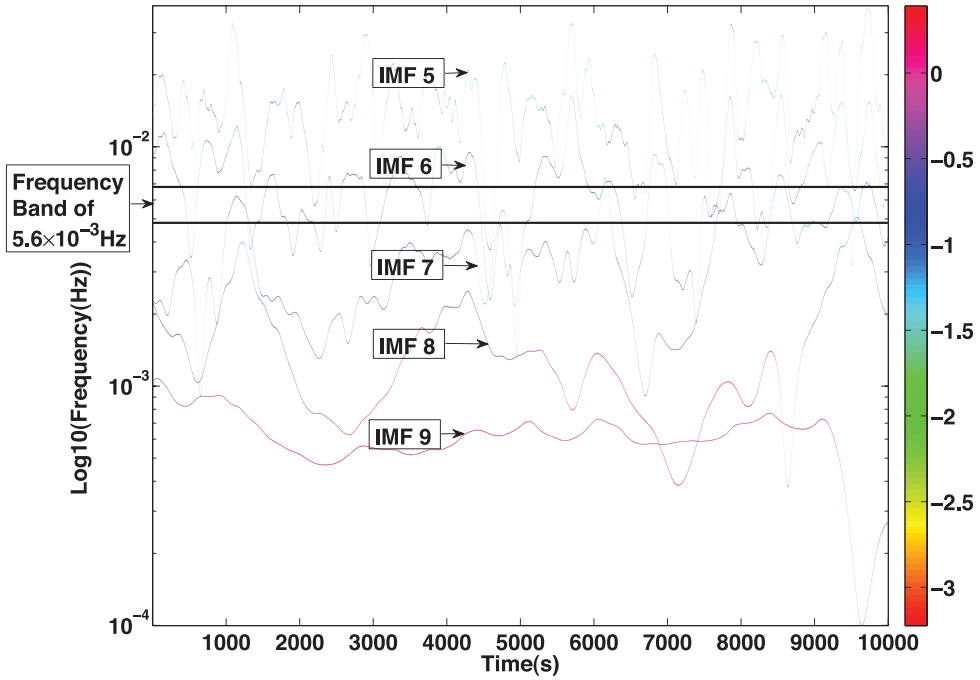

Figure 6. This example illustrates how the frequency estimates ω_0 for the impedance calculation are obtained from instantaneous spectra. One frequency window centered at 5.6×10^{-3} Hz is highlighted as an example. For each time we sample the complex signals of the IMFs that are located within the same window. These are summed up and assigned to the associated center frequency. The IMFs in this figure are obtained from the B_x component used in our synthetic model test.

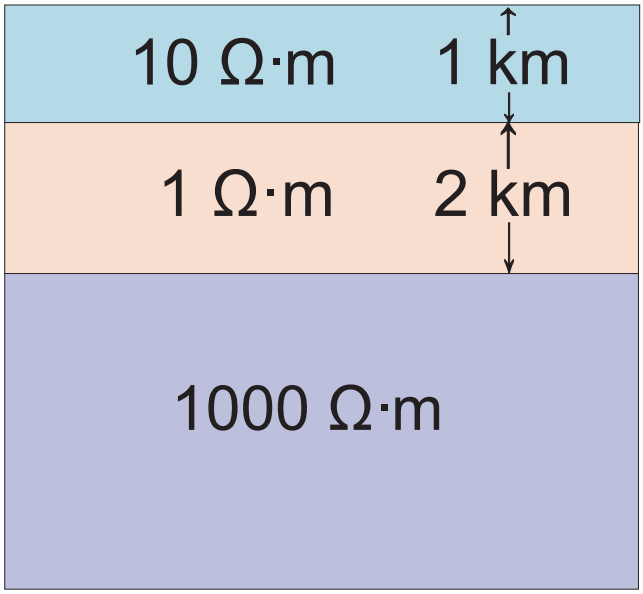

Figure 7. Synthetic layered Earth model to test the new EMD based impedance estimation method. The apparent resistivities and phases determined analytically from the model are shown in Fig. 9 as blue solid lines.

$B_x(\omega)$ to determine $E_x(\omega)$ and $E_y(\omega)$, respectively. Subsequently the electric field spectra are transformed back into time domain to obtain $E_x(t)$ and $E_y(t)$. The synthetic E-field time series are shown in Fig. 8. This construction procedure ensures that classical MT processing methods based on Fourier analysis should recover Z. Note that in this synthetic test all time-series are assumed to be stationary, although we actually want to demonstrate that EMD can also handle non-stationary time-series. The reasons are (i) that it is hard to construct non-stationary time-series for all field components using the Fourier transform and (ii) that we want to be able to compare the results of our new approach with analytic results.

Prior to EMD decomposition we cut both the E- and B-field time-series into 18 short sections with a length of about 12 hr each ($N \approx$ 43 000 samples). This length is comparable to the length of relatively quiet sections measured at station located at the sea-floor, which we will examine later (see also Fig. 12). The number of IMFs we obtained for the different sections varies between 11 and 14. These numbers

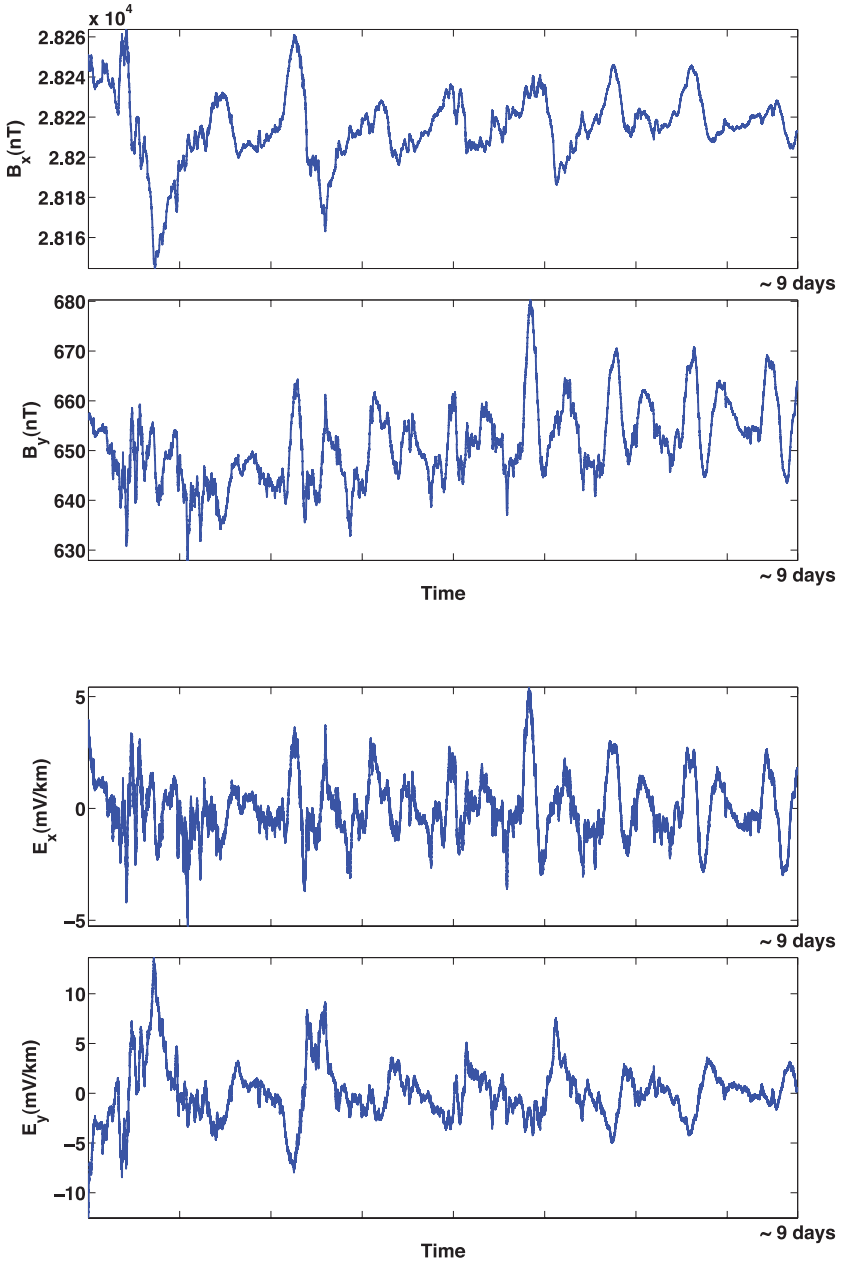

Figure 8. Nine-days long section of B-field data measured onshore Costa Rica in 2007 (above). We use these data as the B-field time-series in our synthetic tests. Synthetic E-field data are constructed from these magnetic field data using the analytically determined impedance $Z(\omega)$ from the layered model shown in Fig. 7.

are slightly smaller than what we would obtain for white noise (∼15) referring to Wu & Huang (2004) and appear to be adequate, because the Fourier spectra of our time-series have a wide spectra relatively close to white noise.

After decomposing each section into IMFs we calculate instantaneous amplitudes and instantaneous frequencies for each IMF. We then divide the spectral range into 25 frequency windows varying from 5.6×10^{-5} Hz to 0.25 Hz, each with identical band-width on a logarithmic scale. For each section the auto- and cross-correlation terms in eq. (13) are calculated. To obtain error estimates we use then the bootstrap method (Efron 1979) to estimate the impedance tensor in each frequency band. Each of the 18 sections is considered as a data point and the number of replications is 200. The mean values obtained by the bootstrapping are considered as the impedance estimates and confidence intervals of 95 per cent are derived from the standard deviations. The estimated apparent resistivity and phase together with their confidence intervals are shown as red circles and error bars in Fig. 9.

While the derived apparent resistivities and phases appear to be reasonable, we observe a small systematic downward bias relative to the analytically determined apparent resistivities. For field data which contains noise, a downward bias in impedance or apparent resistivities derived from eq. (13) is usually observed (Sims *et al.* 1971). The reason is that the denominator in eq. (13) contains an autocorrelation term $\sum_{n=0}^{N} B_{xf}(t_n)B^*_{xf}(t_n) \sum_{n=0}^{N} B_{yf}(t_n)B^*_{yf}(t_n)$, such that noise in the magnetic fields increases the autocorrelation values. The numerator of (13)

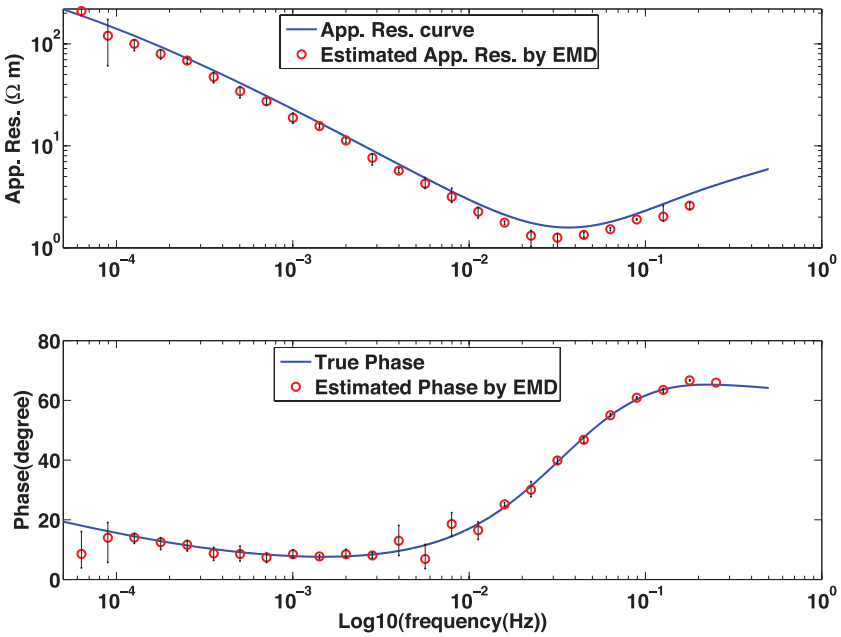

Figure 9. Apparent resistivity (upper panel) and phase (lower panel) estimates from EMD for the synthetic model. Blue curves are the analytic values and red circles are the results from EMD. Note that the apparent resistivities are slightly downward biased.

is less affected by noise, since the cross correlation terms are not systematically changed if the noise in electric and magnetic field data are uncorrelated. Since no measurement noise is present in these synthetically constructed time-series, the downward bias must be introduced by the method itself, that is through the EMD and IF/IA calculation procedures. An analysis of the complete EMD procedure suggests that the introduction of noise occurs through the iterative sifting procedure in the decomposition. Due to the use of a stop criteria and the limited accuracy of the interpolation of the upper and lower envelopes, the subtracted mean is not really the 'true' mean value of the signal. Hence, if this mean is subtracted from the signal, some inaccuracies from the interpolation are added as noise into the signal. After each sifting, these inaccuracies are summed up and create numerical noise in the estimated IMFs.

A downward bias in impedances due to noise on B-field measurements is commonly suppressed by using the remote referencing method (Gamble *et al.* 1979a,b). Remote referencing entails the substitution of the autocorrelation term with a cross correlation term between the magnetic field and a remote reference magnetic field measured in the vicinity of MT site. Assuming that the noise in the magnetic field and the reference magnetic field are uncorrelated, the denominator is then unaffected by noise and the bias vanishes. Since we do not have a 'remote reference' time-series for our synthetic example, we create a 'reference' signal for the impedance calculation by using another algorithm for the decomposition of the same B-field time-series. (To highlight that the reference signal is not taken from another station, we use in the following the term 'numeric reference' instead of 'remote reference'.) So, for the 'numeric reference', the algorithm from Rato *et al.* (2008) and not the one from Huang *et al.* (1998) is used to determine the upper and lower envelopes in the EMD procedure. The algorithm from Rato *et al.* (2008) does not use the actual minima and maxima at the discrete sample positions, but re-positions the extrema by a parabolic interpolation considering amplitudes from one extremum and its two neighboring samples. Because shifting processes are repeated several times for each IMF, introduced numeric inaccuracies are significantly differently distributed over the IMFs for both algorithms. This means that the error contribution in the two final decompositions are mostly uncorrelated for the different frequency bands and the impact of these inaccuracies onto the impedance calculation should be reduced.

To estimate the impedance using the 'numeric' referencing technique, eq. (13) has to be modified to

$$Z_{xy} = \mu_0 \frac{\sum_{n=0}^{N} E_{xf}(t_n) B_{yf}^{r*}(t_n) \sum_{n=0}^{N} B_{xf}(t_n) B_{xf}^{r*}(t_n) - \sum_{n=0}^{N} E_{xf}(t_n) B_{xf}^{r*}(t_n) \sum_{n=0}^{N} B_{xf}(t_n) B_{yf}^{r*}(t_n)}{\sum_{n=0}^{N} B_{xf}(t_n) B_{xf}^{r*}(t_n) \sum_{n=0}^{N} B_{yf}(t_n) B_{yf}^{r*}(t_n) - \sum_{n=0}^{N} B_{xf}(t_n) B_{yf}^{r*}(t_n) \sum_{n=0}^{N} B_{yf}(t_n) B_{xf}^{r*}(t_n)} \tag{14}$$

where $B_{xf}^{r}(t_n)$ and $B_{yf}^{r}(t_n)$ denote the numeric reference time-series. With this procedure we obtain the impedance estimates shown in Fig. 10.

The estimated impedances are now satisfactory although there are still some slight deviations from the analytically determined apparent resistivity curve. These are most likely caused by remaining numerical noise in the empirical mode decomposition and could be improved by using a more sophisticated robust estimation technique. However, this subject is out of the scope of the present paper.

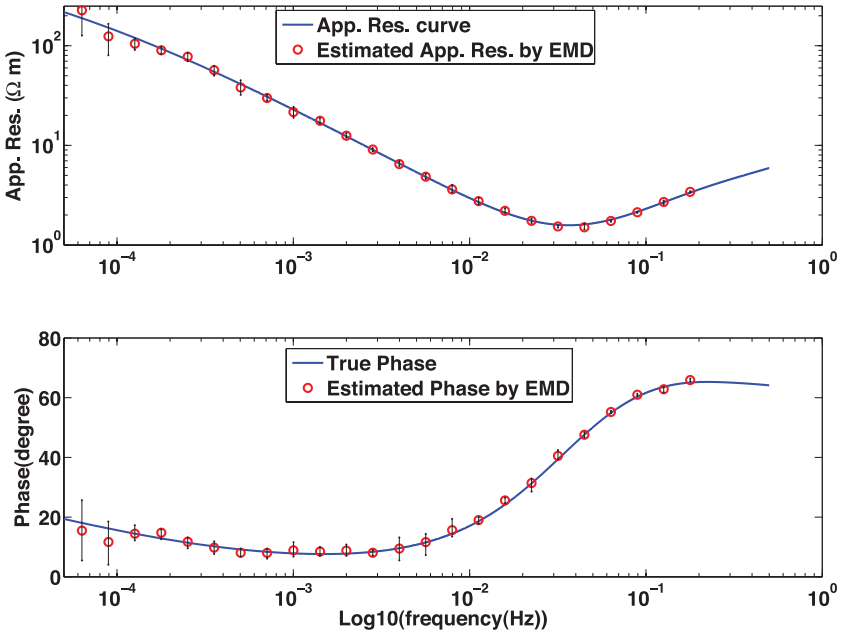

Figure 10. Apparent resistivity (upper panel) and phase (lower panel) estimates from EMD using a 'numeric' reference time-series for the B-field data. For the reference the same B-field data are used as for the original, however, the EMD algorithms applied on the time-series are different. Blue curves are the analytic values and red circles are the estimated results from EMD. Note that the downward bias of apparent resistivities (see Fig. 9) is not present any more.

3.1 Noise test

To investigate how far impedance estimates from our EMD based procedure are affected by noise, we add three different levels of uncorrelated coloured noise to all time-series and repeat the whole procedure to calculate the impedance estimates. In each case, the signal-to-noise ratio is almost the same for all frequencies in order to make it easier to evaluate how the impedance estimation procedure treats noise in the different frequency ranges.

To determine the noise contributions, we first smooth the Fourier amplitude spectra of the time-series from all field components and take ∼2 per cent, ∼5 per cent and ∼10 per cent of all amplitude spectra as the noise levels. Randomized phase spectra are then added to the amplitude spectra and the entire noise sequence is transferred back to the time domain. We check that all noise sequences are uncorrelated before we finally add them to the corresponding time-series of the different field components. Apparent resistivity and phase estimates for noise levels of 2 per cent, 5 per cent and 10 per cent are presented in the Fig. 11. In addition to our EMD based procedure we also determine estimates from the simple Fourier derived impedance formula (eq. 10) and the robust processing method BIRRP (Chave & Thomson 2004). For the simple Fourier based estimates we use the same window length as for the EMD procedure. To make the results more stable the linear trends in the time-series are removed and Hanning windows are applied before the Fourier transforms are performed. For EMD and for the simple Fourier based estimates we performed the bootstrapping strategy as described above to get estimates for the error variances.

Mean values from the EMD and simple Fourier derived impedance formula fit similarly well for low frequencies in the apparent resistivity and phase estimates. However, for higher frequencies the mean values from the EMD often fit better than the ones from simple Fourier based formula and the error variances are typically smaller. The results from the EMD are typically in a similar range or slightly worse than for the robust processing method BIRRP. In particular, for the phase we obtain less precise estimates from the EMD than from BIRRP for all three noise levels.

Comparison of the results from the different methods demonstrates that EMD provides reliable impedance estimates and we conclude that the EMD procedure has the potential to handle noisy data sets. Note that in the EMD procedure no robust processing steps are implemented yet and accordingly one would expect that EMD results should be comparable to those of the simple Fourier derived impedance formula. However, results from the EMD procedure are better. This is most likely due to the facts, that (i) noise added to the data acts locally for EMD processing and is not, as in the Fourier approach, smeared over different frequencies and (ii) while the noise that has been added to the data is stationary over the entire time-series, cutting the time-series into segments may introduce non-stationary effects for the shorter time segments.

4 REAL MARINE MT DATA FROM COSTA RICA

We now apply our newly developed method to MT data recorded offshore Costa Rica (Worzewski *et al.* 2011). These data are strongly influenced by instrument tilt caused by wave motion, which makes large parts of the data unusable for processing with traditional estimation methods. MT data were collected for total 11 stations in 2007 along a profile across the Costa Rica subduction zone (Fig. 12). At each station

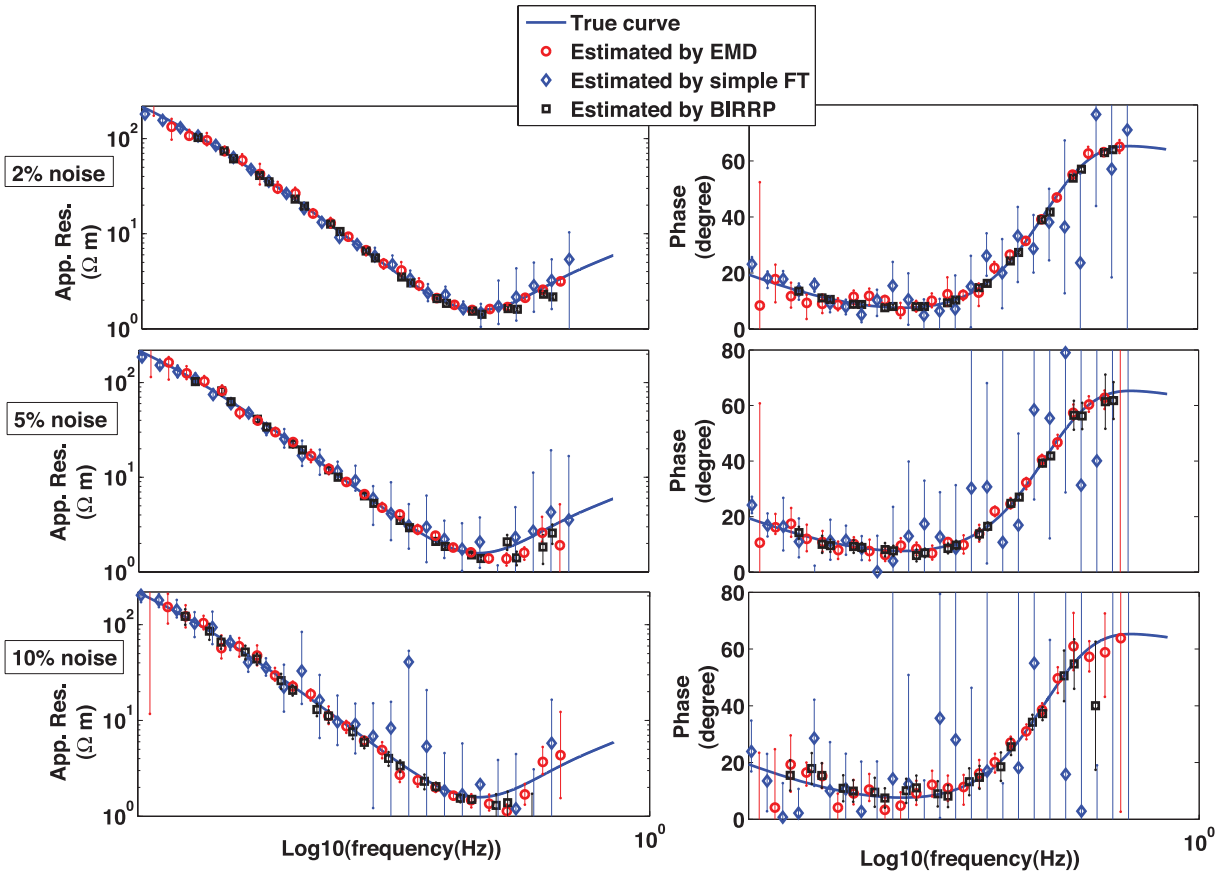

Figure 11. Apparent resistivity (left panels) and phase (right panels) estimates from EMD using a 'numeric' reference time-series for the B-field data. In contrast to Fig. 10 uncorrelated coloured noises of different levels are added to all time-series. From top to bottom, the amount of noise corresponds to ∼2 per cent, ∼5 per cent and ∼10 per cent of the amplitude spectra of the associated time-series. In addition to the estimates from EMD (red circles), estimates from Fourier transform without any robust processing steps (blue diamonds) and estimates from BIRRP (black square) are presented.

we measured three components of the magnetic field, two horizontal electric field components and two components of the tilt movement with a sampling rate of 1 Hz. At the same time the three magnetic field components were recorded at a reference station on land.

Depending on their position, the marine MT stations are influenced by motion induced noise of varying degrees. The station closest to shore, station 1, shows such strong noise that we could not obtain any impedance estimates with any processing technique. The station furthest from the coast, station 11, shows only intermittent tilt movement and has the longest quiet sections of all stations in the profile, as shown in Fig. 13. We will use this station to demonstrate our processing method below. As it is located in 3105 m deep water, the high frequencies are strongly attenuated and it is difficult to estimate the impedance for frequencies larger than 0.03 Hz. We show the longest quiet electric and magnetic time-series for station 11 in Fig. 14, and the simultaneously measured magnetic time-series for reference land station in Fig. 15.

From Fig. 13 we can see that the length of the quiet sections varies between 8 hr and 23 d. For our processing we only use the quiet sections that are associated with weak tilt movements. Longer quiet sections are, moreover, cut into shorter sections of up to 24 hr length for the empirical mode decomposition in order to save computation time. This results in a total of 35 sections. We divide the frequency range between 5.6×10^{-5} Hz and 0.2 Hz into 24 bands with equal width on a logarithmic scale. Similar to the synthetic example above, we apply EMD to all electric and magnetic field components of the marine station and the magnetic field components of the reference land station. From the calculated IMFs, we compute instantaneous spectra and sum up contributions using eq. (14) for times at which the instantaneous spectra of all components fall in the same frequency band as outlined above. The whole computation time is approximately 6 hr using a 3.2 GHz computer with 2 CPUs. The error bars are estimated using the bootstrap method and constitute a 95 per cent confidence interval in the same manner as used for the synthetic model. We show the obtained apparent resistivity and phase curves for the two off-diagonal components in Fig. 16 together with the results obtained by BIRRP.

Although we do not use any robust estimation or other sophisticated fitting procedure as in BIRRP, our results are satisfactory and comparable to the results obtained with BIRRP. Furthermore, apart from cutting out the noisy sections, we have not preprocessed or filtered the data in any way. Even though some work remains to be done, these first results demonstrate that EMD technique is a suitable alternative processing method for MT data.

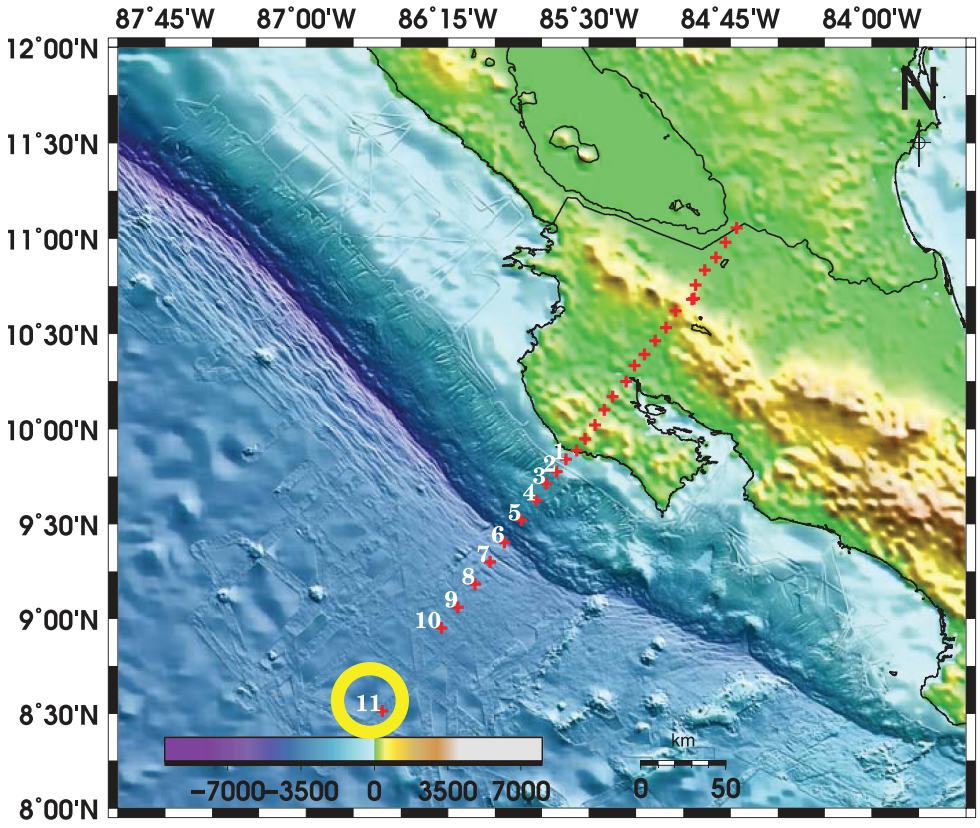

Figure 12. Topographic map and MT profile across the Costa Rican subduction zone. Offshore MT stations were deployed by GEOMAR, Kiel, in 2007 and land stations were installed by the Free University of Berlin in 2008. As an example, data of the marine station 11 highlighted by the yellow circle is used for comparison of BIRRP and EMD processing (see Fig. 16).

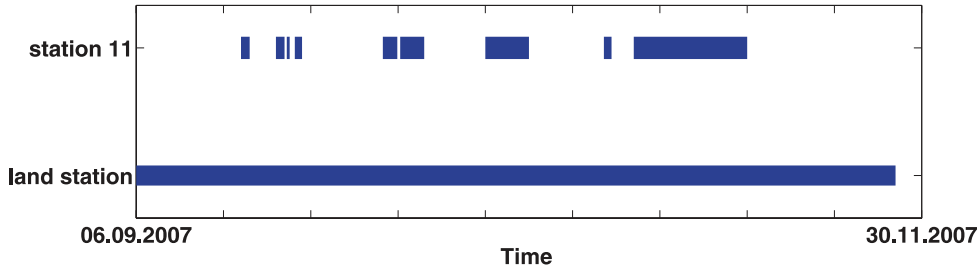

Figure 13. Blue bars denote periods where no significant noise is present in the electromagnetic time-series. While the land station data does not exhibit significant noise over the entire measuring period, marine MT data at station 11 is affected by motion induced tilt variations.

5 CONCLUSION AND OUTLOOK

In this paper we show that EMD is a viable alternative for processing MT data and can be used to obtain frequency dependent impedance tensors estimates from electric and magnetic field time-series. EMD adaptively decomposes a time-series into a number of mono-component basis functions and allows the calculation of physical meaningful instantaneous frequencies and spectra at every time sample. The method is not based on the assumption that the recorded electromagnetic fields are stationary as is the case for a Fourier based technique. Therefore, it is applicable on data with any degree of non-stationarity and has the potential to be an alternative MT processing technique when other methods fail.

By means of synthetic tests on a 1-D model we illustrate how this decomposition can be practically implemented. Results demonstrate that the apparent resistivities and phase estimates derived from this impedance tensor are generally stable. However, systematic downward shifts are present in the final apparent resistivity estimates. We associate these downward shifts with numerical noise that is introduced by the decomposition and we find that the shifts can be strongly reduced by applying a second EMD algorithm to create a numerical reference time-series of the B-field. From additional synthetic tests we conclude that our EMD based procedure provides similar or even better results than simple Fourier derived impedance formulas in the presence of stochastic noise. However, when compared to impedances determined using the robust processing method BIRRP, the results are slightly worse. This is to be expected as our implementation of EMD does not

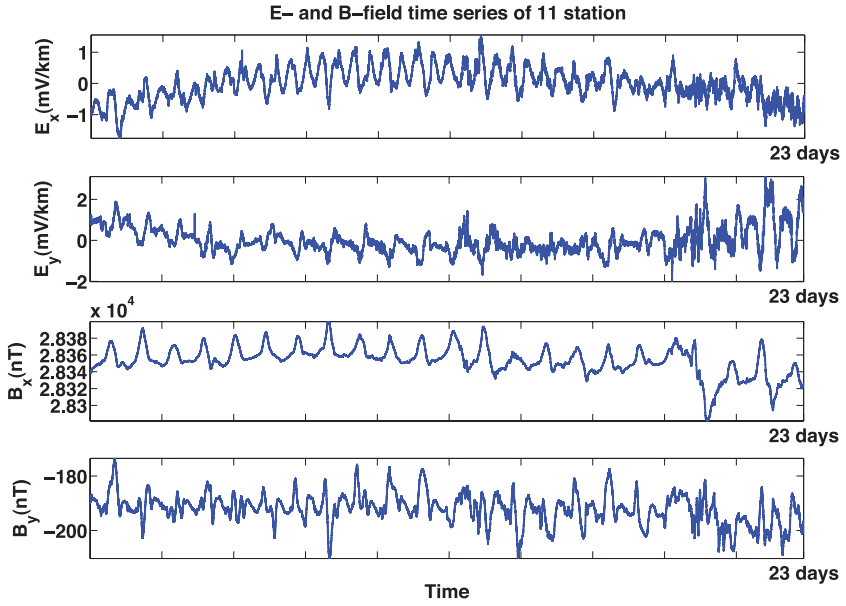

Figure 14. One long quiet section of E- and B-field time-series at MT station 11 in Costa Rica (sampling frequency is 1 Hz).

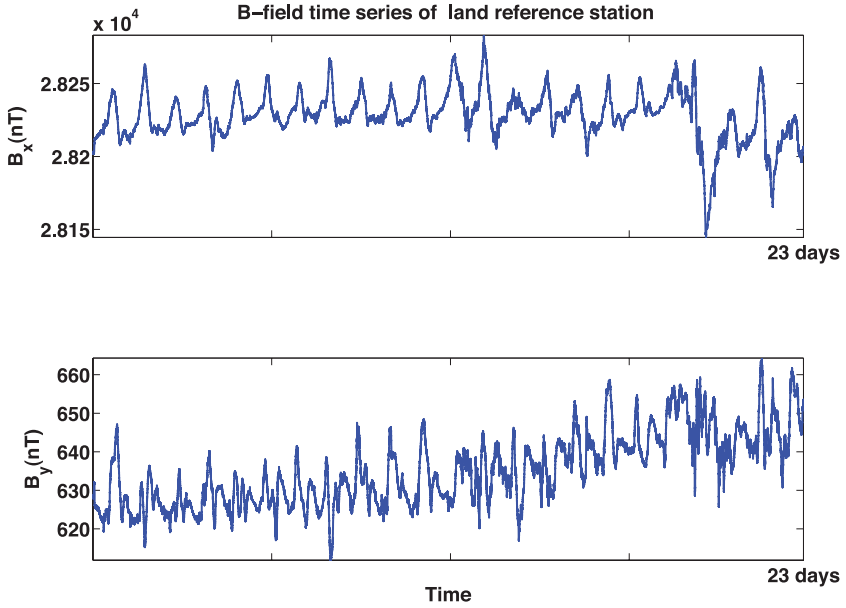

Figure 15. B-field time-series from a land station that we use as the remote reference site. The time window shown here corresponds to the quiet section shown in Fig. 14.

include robust processing techniques at the present stage. For our tests on real data the impedance estimates from the EMD method and BIRRP are very similar, indicating that EMD method is suitable for practical applications.

The next logical step is to combine robust processing procedures, such as those employed in BIRRP, together with the EMD processing method in order to make impedance estimates less sensitive to noise. This will take this research from a proof of principle analysis to a stage where it can be used in practise. In addition, EMD may have the potential to remove noise which is present in specific frequency ranges at an earlier stage of the MT processing. In conventional approaches, entire sections in a time-series often must be removed prior to processing, due to severe non-stationarity in the recorded data. However, with the EMD method, part of these sections could still be preserved for the IMFs which contain little noise. One of the practical implications for such a noise removal procedure could be in marine MT processing, where the recorded magnetic field is often contaminated with high frequency noise caused by instrument motion due to deep water or tidal currents.

ACKNOWLEDGMENTS

This publication is contribution no. 243 of the Sonderforschungsbereich 574 ‘Volatiles and Fluids in Subduction Zones’ at Kiel University. The EMD Matlab codes used in this paper are modified from P. Flandrin of Laboratoire de Physique CNRS & ENS Lyon (France): http://perso.ens-lyon.fr/patrick.flandrin/emd.html. Special thanks to Andrei Swidinsky for fruitful comments and correction of the language.

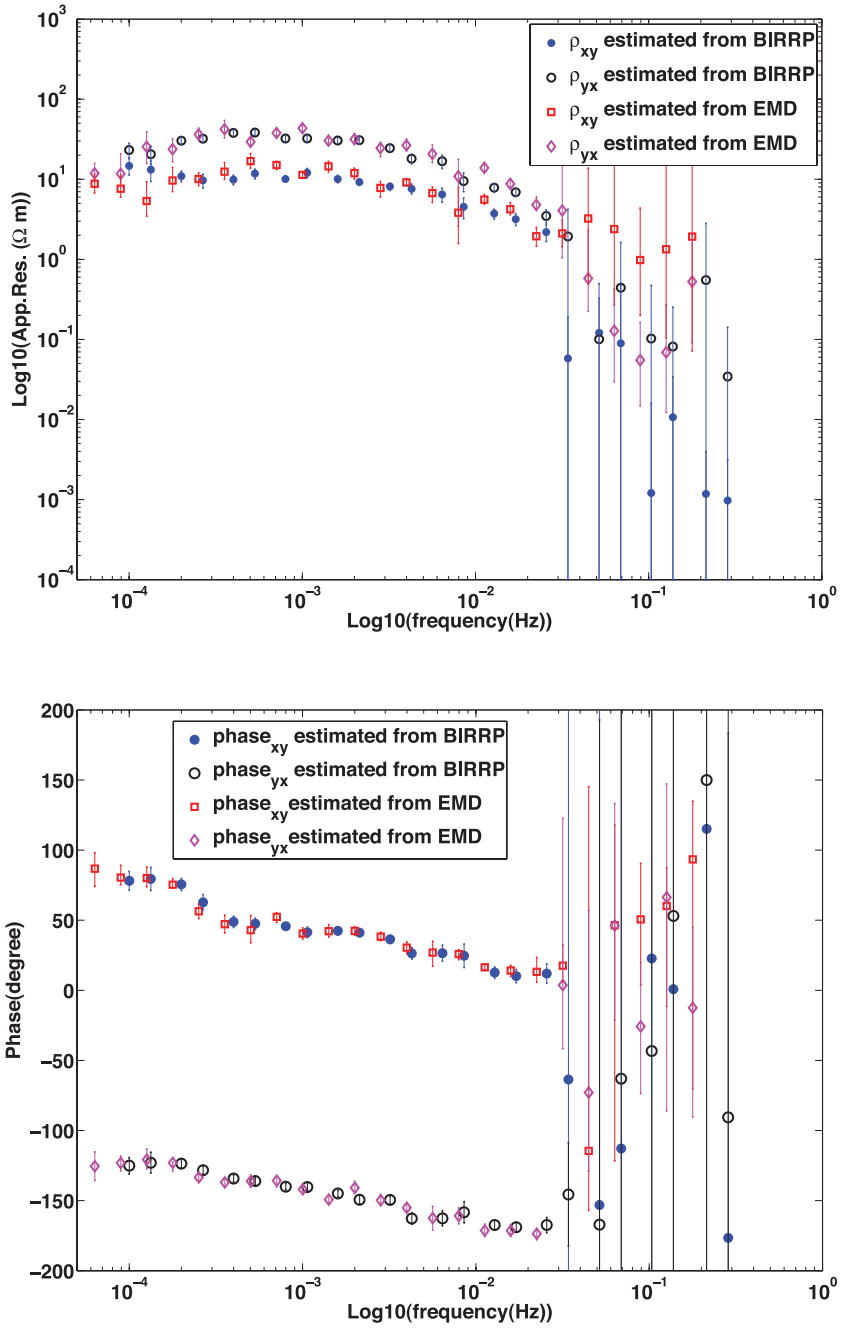

Figure 16. Comparison of results derived from BIRRP processing and EMD processing. Upper panel: off-diagonal apparent resistivities, blue dots and black circles indicate the results from BIRRP, red square and magenta diamonds from EMD. Lower panel: phase, blue dots and black circles indicate the results from BIRRP, red square and magenta diamonds from EMD.

We are also thankful for very helpful discussions with Andreas Junge, Gary Egbert, Maik Neukirch and Pierre Wawrzyniak. Comments and corrections from the two reviewers, Alan Chave and Xavier Garcia, helped us to significantly improve the manuscript.

REFERENCES

Alexandrescu, M., Gilbert, D., Hulot, G., Le Mouel, J.-L. & Saracco, G., 1995. Detection of geomagnetic jerks using wavelet analysis, *J. geophys. Res.,* **100,** 12 557–12 572.

Bedrosian, E., 1963. A product theorem for Hilbert transforms, *Proc. IEEE,* **51**(5), 868–869.

Berdichevsky, M.N., 1973. Magnetotelluric sounding with applications to mathematical filters, *Phys. Earth,* **3,** 76–92.

Boashash, B., 1992a. Estimating and interpreting the instantaneous frequency of a signal–part 1: fundamentals, *Proc. IEEE,* **80**(4), 520–538.

Boashash, B., 1992b. Estimating and interpreting the instantaneous frequency of a signal–part 2: algorithms and applications, *Proc. IEEE,* **80**(4), 540–568.

Chant, I.J. & Hastie, L.M., 1992. Time-frequency analysis of magnetotelluric data, *Geophys. J. Int.,* **111,** 399–413.

Chant, I.J. & Hastie, L.M., 1993. A comparison of the stability of stationary and non-stationary magnetotelluric analysis methods, *Geophys. J. Int.,* **115,** 1143–1147.

Chave, A.D. & Thomson, D.J., 1989. Some comments on magnetotelluric response function estimation, *J. geophys. Res.,* **94**(B10), 14 215–14 225.

Chave, A.D. & Thomson, D.J., 2004. Bounded influence magnetotelluric response function estimation, *Geophys. J. Int.,* **157,** 988–1006.

Chave, A.D., Thomson, D.J. & Ander, M.E., 1987. On the robust estimation of power spectra, coherences, and transfer functions, *J. geophys. Res.,* **92**(B1), 633–648.

Duffy, D.G., 2004. The application of Hilbert-Huang transforms to meteorological data sets, *J. Atmos. Oceanic Technol.,* **21,** 599–611.

Efron, B., 1979. Bootstrap methods: another look at the jackknife, *Annal. Stat.,* **7**(1), 1–26.

Egbert, G.D., 1997. Robust multiple-station magnetotelluric data processing, *Geophys. J. Int.,* **130,** 475–496.

Egbert, G.D. & Booker, J.R., 1986. Robust estimation of geomagnetic transfer functions, *Geophys. J. R. astr. Soc.,* **87,** 173–194.

Flandrin, P., 1999. *Time-Frequency/Time-Scale Analysis,* Academic Press, San Diego, CA.

Flandrin, P., 2004. Empirical mode decompositions as data-driven wavelet-like expansions, *Int. J. Wavelets, Multires. Infor. Proc.,* **2**(4), 1–20.

Gabor, D., 1946. Theory of communication, *J. IEE,* **93,** 429–457.

Gamble, T., Goubau, W. & Clarke, J., 1979a. Magnetotellurics with a remote magnetic reference, *Geophysics,* **44,** 53–68.

Gamble, T., Goubau, W. & Clarke, J., 1979b. Error analysis for remote reference magnetotellurics, *Geophysics,* **44,** 959–968.

Garcia, X. & Jones, A., 2008. Robust processing of magentotelluric data in the amt dead band using the continuous wavelet tranform, *Geophysics,* **73**(6), F223–F234.

Huang, N. *et al.*, 1998. The empirical mode decomposition and the Hilbert spectrum for nonlinear and non-stationary time series analysis, *Proc. R. Soc. Lond. A,* **454,** 903–995.

Huang, N.E., Chern, C.C., Huang, K., Long, L.W.S.S.R. & Fan, K.L., 2001. A new spectral representation of earth-quake data: Hilbert spectral analysis of station TCU129, Chi-Chi, Taiwan, 21 September 1999, *Bull. seism. Soc. Am.,* **91,** 1310–1338.

Huang, T., Ren, W. & Lou, M., 2008. The orthogonal Hilbert-Huang transform and its application in earthquake motion recordings analysis, in *Proceedings of the 14th World Conference on Earthquake Engineering, October 12–17, 2008, Bejing, China*.

Huang, N.E. & Wu, Z., 2008. A review on Hilbert-Huang transform: method and its applications to geophysical studies, *Rev. Geophys.,* **46**(RG2006), 23, doi:10.1029/2007RG000228.

Huang, N.E., Wu, Z. & Long, S.R., 2009. On instantaneous frequency, *Adv. Adapti. Data Anal.,* **1**(2), 177–229.

Junge, A., 1996. Characterization of and correction for cultural noise, *Surveys Geophy.,* **17,** 361–391.

Lamarque, G., 1999. Improvement of MT data processing using stationary and coherence tests, *Geophys. Prospect.,* **47,** 819–840.

Loughlin, P.J. & Tracer, B., 1996. On the amplitude and frequency-modulation decomposition of signals, *J. acoust. Soc. Am.,* **100,** 1594–1601.

Nuttall, A.H. & Bedrosian, E., 1966. On the quadrature approximation to the Hilbert transform of modulated signals, *Proc. IEEE,* **54**(10), 1458–1459.

Qian, W. & Pedersen, L.B., 1991. Industrial interference magnetotellurics: an example from the Tangshan area, China, *Geophysics,* **56,** 265–273.

Rato, R.T., Ortigueira, M.D. & Batista, A.G., 2008. On the hht, its problems, and some solutions, *Mech. Syst. Signal Process.,* **22,** 1374–1394.

Rilling, G., Flandrin, P. & Goncalves, P., 2003. On empirical mode decomposition and its algorithms, in *Proceedings of the 6th IEEE/EURASIP Workshop on Nonlinear Signal and Image Processing(NSIP '03),* Grado, Italy.

Sims, W., Bostick, F. & Smith, H., 1971. The estimation of magnetotelluric impedance tensor elements from measured data, *Geophysics,* **36,** 938–942.

Spagnolini, U., 1994. Time domain estimation of MT impedance tensor, *Geophysics,* **59,** 712–721.

Sutarno, D. & Vozoff, R., 1991. Phase-smoothed robust M-estimation of magnetotelluric impedance functions, *Geophysics,* **56,** 1999–2007.

Suto, N., Harada, M., Izutsu, J. & Nagao, T., 2006. Time variation of the electromagnetic transfer function of the earth estimated by using wavelet transform, *Proc. Jpn. Acad., Ser. B,* **82,** 175–180.

Szarka, L., 1988. Geophysical aspects of man-made electromagnetic noise in the earth - a review, *Surveys Geophys.,* **9,** 287–318.

Thomson, D.J., 1982. Spectrum estimation and harmonic analysis, *Proc. IEEE,* **70,** 1055–1096.

Vasudevan, K. & Cook, F.A., 2000. Empirical mode skeletonization of deep crustal seismic data: therory and applications, *J. geophys. Res.,* **105,** 7845–7856.

Vozoff, K., 1972. The magnetotelluric method in the exploration of sedimentary basins, *Geophysics,* **37,** 98–141.

Worzewski, T., Jegen, M., Kopp, H., Brasse, H. & Castillo, E.T., 2011. Magnetotelluric image of the fluid cycle in the Costa Rican subduction zone, *Nature Geosci.,* **4,** 108–111.

Wu, Z. & Huang, N.E., 2004. A study of the characteristics of white noise using the empirical mode decomposition method, *Proc. R. Soc. Lond. A,* **460,** 1597–1611.

Zhang, R.R., 2006. Characterizing and quantifying earthquake-induced site nonlinearity, *Soil Dyn. Earthquake Eng.,* **26,** 799–812.

Zhang, R.R., Ma, S. & Hartzell, S., 2003a. Signatures of the seismic source in end-based characterization of the 1994 north-ridge, California, earthquake recordings, *Bull. seism. Soc. Am.,* **93,** 501–518.

Zhang, R.R., Ma, S., Safak, E. & Hartzell, S., 2003b. Hilbert-Huang transform analysis of dynamic and earthquake motion recordings, *J. Eng. Mech.,***129,** 861–875.